

Pure moving optical media consisting of magnetochiral metasurfaces

TOSHIYUKI KODAMA,^{1,*} TOSHIHIRO NAKANISHI,² KEI SAWADA,^{3,4} AND SATOSHI TOMITA^{1,5,†}

¹ *Institute for Excellence in Higher Education, Tohoku University, Sendai 980-8576, Japan*

² *Division of Electronic Science and Engineering, Graduate School of Engineering, Kyoto University, Kyoto 615-8515, Japan*

³ *RIKEN SPring-8 Center, Sayo, Hyogo 679-5148, Japan*

⁴ *Cornell High Energy Synchrotron Source, Cornell University, Ithaca, NY 14853, USA*

⁵ *Department of Physics, Graduate School of Science, Tohoku University, Sendai 980-8578, Japan*

*tkodama@tohoku.ac.jp

†tomita@tohoku.ac.jp

Abstract: We report numerical studies of microwave bianisotropies by magnetochiral (MCh) metasurfaces consisting of double Z-type gammadions with perpendicularly magnetized substrates. The metasurfaces' effective polarizability tensor, extracted from calculated reflection and transmission coefficients, has components of the non-reciprocal moving-type bianisotropy as well as the reciprocal chiral-type bianisotropy and non-reciprocal magneto-optical (MO) effect. Combination of the metasurfaces with contraposition MCh metasurfaces cancels both the chiral-type bianisotropy and MO effect, resulting in pure moving optical media. Achieved perfect transmission with phase difference of π realizes an ideal gyrotator for arbitrary spatial and polarization modes.

1. Introduction

Symmetries relate to laws in optics. Noether's theorem says that a system with a continuous symmetry has a conserved quantity; for example, the frequency (energy) of light is conserved in a medium with the time-translational symmetry. Another kind of symmetries is a discrete one, such as the spatial-inversion and time-reversal symmetry. These symmetries impose restrictions on optical phenomena and play essential roles in optics [1]. A breaking of the space-inversion and/or time-reversal symmetry gives rise to bianisotropies [2,3], which represent cross-correlated electromagnetic inductions among electric polarizability, magnetization, and electromagnetic fields i.e., magnetoelectric couplings, in constitutive equations. The bianisotropies are classified into the four categories associated with reciprocity and polarization dependence as follows [4]: a reciprocal chiral-type bianisotropy with polarization plane rotation, a reciprocal omega-type without polarization rotation, a non-reciprocal Tellegen-type with polarization rotation, and a non-reciprocal moving-type without polarization rotation. The control of the bianisotropies is a challenge in natural materials with broken symmetries such as multiferroic materials [5–7]; therefore, man-made structured materials, referred to as metamaterials, are suitable to explore bianisotropies [8–12]. In particular, metasurfaces with two-dimensional planar structures are good playgrounds to embody a tailor-made bianisotropic medium [13–16].

In this work, we theoretically and numerically study magnetochiral (MCh) metasurfaces as non-reciprocal moving-type bianisotropic media. The MCh metasurfaces consist of double Z-type gammadion with the broken space-inversion symmetry [17] and perpendicularly magnetized substrate with the broken time-reversal symmetry. The optical MCh effect [18–34] is manifested in a transmission coefficient difference, which is dependent on propagation direction but independent of polarization, due to the moving-type bianisotropy. We calculate transmission and reflection coefficient spectra at normal incidence of microwaves to evaluate effective polarizability tensor [35–37]. The effective polarizability tensor demonstrates the moving-type

bianisotropy as well as the chiral-type bianisotropy and magneto-optical (MO) effect. Furthermore, a composite metasurface consisting of the ordinary and contraposition MCh metasurfaces realizes pure moving optical media without optical activity and MO effect. The pure moving media show the perfect transmission with a phase difference of π depending on propagation direction, bringing about an ideal gyrator [38].

The pure moving optical media are of great interest in terms of development of functional metasurfaces. A similar story can be found in the development of the well-known negative refractive index metamaterials consisting of split-ring resonators (SRRs). A single C-shaped SRR shows the omega-type bianisotropy due to electromagnetic interaction in addition to magnetic permeability [39, 40]. This brings about electromagnetic responses not only to magnetic field but also to electric field. An inverse-C-shaped SRR is thus incorporated in the inner circle of the C-shaped SRR, resulting in vanishment of the omega-type electromagnetic interaction but remaining of the permeability component. This way, the double SRRs construct pure negative magnetic permeability media, bringing about negative refractive index metamaterials. Similarly, the pure moving medium without the optical activity and MO effect obtained in this study is a key to realize an ideal gyrator for arbitrary spatial and polarization modes.

This paper is organized in five sections. Section 2 details theoretical background, including effective polarizability tensor, principle of parameter retrieving, and classification of bianisotropic metasurfaces. Section 3 devotes to numerical calculation setup. Section 4 describes results and discussion of calculated microwave transmission and reflection coefficient spectra of the uniaxial bianisotropic MCh metasurfaces. The extracted effective polarizability tensor of the chiral and MCh metasurfaces is illustrated. We present pure moving optical media by introducing contraposition MCh metasurfaces with the inverse chirality and converse magnetization of the ordinary MCh metasurfaces. The pure moving media result in perfect transmission and phase difference of π . Section 5 concludes the paper.

2. Theoretical background

2.1. Effective polarizability tensor

The electromagnetic properties of a metasurface, which interacts with normally incident plane waves propagating in the $+z$ direction, can be fully characterized by the following effective polarizability tensor $\hat{\alpha}_{ij}$ defined as

$$\begin{pmatrix} P_x \\ P_y \\ M_x \\ M_y \end{pmatrix} = \begin{pmatrix} \hat{\alpha}_{xx}^{ee} & \hat{\alpha}_{xy}^{ee} & \hat{\alpha}_{xx}^{em} & \hat{\alpha}_{xy}^{em} \\ \hat{\alpha}_{yx}^{ee} & \hat{\alpha}_{yy}^{ee} & \hat{\alpha}_{yx}^{em} & \hat{\alpha}_{yy}^{em} \\ \hat{\alpha}_{xx}^{me} & \hat{\alpha}_{xy}^{me} & \hat{\alpha}_{xx}^{mm} & \hat{\alpha}_{xy}^{mm} \\ \hat{\alpha}_{yx}^{me} & \hat{\alpha}_{yy}^{me} & \hat{\alpha}_{yx}^{mm} & \hat{\alpha}_{yy}^{mm} \end{pmatrix} \begin{pmatrix} E_x^{\text{inc}} \\ E_y^{\text{inc}} \\ H_x^{\text{inc}} \\ H_y^{\text{inc}} \end{pmatrix}, \quad (1)$$

where the superscript e and m in $\hat{\alpha}_{ij}$ are assigned to electric and magnetic stimulus/responses, respectively. The subscript $i = x, y$ ($j = x, y$) in $\hat{\alpha}$ represents the polarization direction of the output (input) waves. The i components ($i = x, y$) of induced electric moment per a unit area, induced magnetic moment per a unit area, incident electric field, and incident magnetic field, are represented respectively by P_i , M_i , E_i^{inc} , and H_i^{inc} [3]. In this way, $\hat{\alpha}_{xy}^{em}$, for example, represents an effective polarizability tensor element, where a magnetic field in the y direction induces an electric dipole moment in the x direction. General metasurfaces with anisotropic magneto-electric interactions are referred to as bianisotropic metasurfaces.

Here we write the plane waves to be, $E, H \propto e^{j(-\vec{k}\cdot\vec{r}+\omega t)}$, where $j = \sqrt{-1}$ is the imaginary unit. In this notation, the effective polarizability tensor components can be expressed in a

non-dimensional manner to be

$$\alpha_{xx}^{ee}\omega Z_0 = \frac{j}{2}(t_{xx}^+ + t_{xx}^- + r_{xx}^+ + r_{xx}^- - 2), \quad (2)$$

$$\alpha_{yy}^{mm}\omega Z_0^{-1} = \frac{j}{2}(t_{xx}^+ + t_{xx}^- - r_{xx}^+ - r_{xx}^- - 2), \quad (3)$$

$$\alpha_{xy}^{em}\omega = \frac{j}{2}(t_{xx}^+ - t_{xx}^- + r_{xx}^+ - r_{xx}^-), \quad (4)$$

$$\alpha_{yx}^{me}\omega = \frac{j}{2}(t_{xx}^+ - t_{xx}^- - r_{xx}^+ + r_{xx}^-), \quad (5)$$

$$\alpha_{yx}^{ee}\omega Z_0 = \frac{j}{2}(t_{yx}^+ + t_{yx}^- + r_{yx}^+ + r_{yx}^-), \quad (6)$$

$$\alpha_{xy}^{mm}\omega Z_0^{-1} = -\frac{j}{2}(t_{yx}^+ + t_{yx}^- - r_{yx}^+ - r_{yx}^-), \quad (7)$$

$$\alpha_{yy}^{em}\omega = \frac{j}{2}(t_{yx}^+ - t_{yx}^- + r_{yx}^+ - r_{yx}^-), \quad (8)$$

$$\alpha_{xx}^{me}\omega = -\frac{j}{2}(t_{yx}^+ - t_{yx}^- - r_{yx}^+ + r_{yx}^-), \quad (9)$$

with transmission coefficients t_{ij}^\pm and reflection coefficients r_{ij}^\pm , where the superscript \pm represents the sign of z component of the wavevector [37]. A wave impedance of a vacuum is represented by Z_0 . The above components are derived from the transmission and reflection coefficients for x -polarized incident waves, i.e. t_{ix}^\pm, r_{ix}^\pm ($i = x, y$). The effective polarizabilities given by Eqs. (2) to (5) are related to polarization-maintaining interaction, while those given by Eqs. (6) to (9) are related to interaction involving polarization conversion from x -polarized waves to y -polarized waves. The remaining components can be calculated from the transmission and reflection coefficients for the y -polarized incident waves, i.e. t_{iy}^\pm, r_{iy}^\pm ($i = x, y$).

Suppose a uniaxial metasurface with the z -axis rotational symmetry. The following relations hold: $t_{xx}^\pm = t_{yy}^\pm, r_{xx}^\pm = r_{yy}^\pm, t_{xy}^\pm = -t_{yx}^\pm, r_{xy}^\pm = -r_{yx}^\pm$, which yield $\hat{\alpha}_{xx}^{ee} = \hat{\alpha}_{yy}^{ee}, \hat{\alpha}_{xx}^{mm} = \hat{\alpha}_{yy}^{mm}, \hat{\alpha}_{xy}^{em} = -\hat{\alpha}_{yx}^{em}, \hat{\alpha}_{yx}^{me} = -\hat{\alpha}_{xy}^{me}, \hat{\alpha}_{yx}^{ee} = -\hat{\alpha}_{xy}^{ee}, \hat{\alpha}_{xy}^{mm} = -\hat{\alpha}_{yx}^{mm}, \hat{\alpha}_{yy}^{em} = \hat{\alpha}_{xx}^{em}, \hat{\alpha}_{xx}^{me} = \hat{\alpha}_{yy}^{me}$. As a result, the uniaxial metasurface is fully characterized by the components of the effective polarizability tensor given by Eq. (2) to Eq. (9). In this paper, we evaluate these effective polarizabilities using transmission and reflection coefficients from numerically calculated S parameters of the MCH metasurfaces.

2.2. Principle of parameter retrieving

We provide physical insights into the parameter retrieving given by Eqs. (2) to (9). For sake of simplicity, the case without polarization rotation is considered; $t_{xy}^\pm = t_{yx}^\pm = r_{xy}^\pm = r_{yx}^\pm = 0$. Moreover, we simplify as $t^\pm = t_{xx}^\pm$ and $r^\pm = r_{xx}^\pm$. Figures 1(a) and 1(b) illustrate electromagnetic responses by incident waves propagating in the positive and negative direction, respectively. Electromagnetic waves in Figs. 1(a) and 1(b) can be regarded as superpositions of incident waves and scattered waves S_l^\pm ($l = f, b$) radiated by electric and/or magnetic responses of the metasurface as shown in Figs. 1(c) and 1(d). The superscript, \pm , represents the direction of the incident waves, and S_f^\pm (S_b^\pm) represents the scattered waves propagating forward (backward) with respect to the incident waves. Comparing Figs. 1(a) (b) and (c) (d), we obtain

$$t^\pm = 1 + S_f^\pm, \quad (10)$$

$$r^\pm = S_b^\pm. \quad (11)$$

On the metasurface, electric and magnetic fields coexist for one-way propagating waves. Nevertheless, either the electric fields or magnetic fields can be zero by destructive interference between plane waves with opposite propagation directions, which form standing waves. For

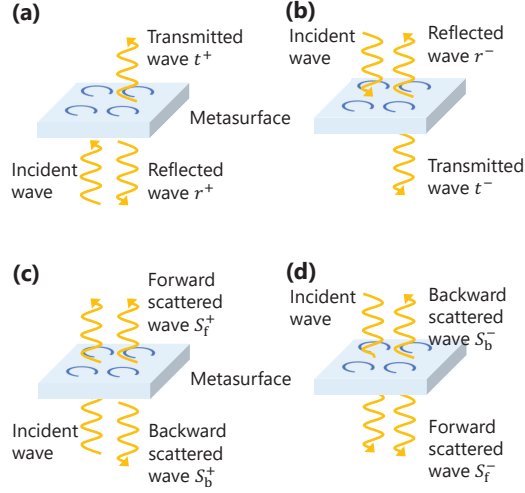


Fig. 1. (a) A transmitted wave t^+ and reflected wave r^+ by the incident wave in the positive direction (+). (b) A transmitted wave t^- and reflected wave r^- by the incident wave in the negative direction (-). (c) Redrawn of (a) using the forward scattered wave S_f^+ and the backward scattered wave S_b^+ . (d) Redrawn of (b) using the forward scattered wave S_f^- and the backward scattered wave S_b^- .

example, when electromagnetic waves with in-phase electric fields propagating in opposite directions are incident on the metasurface, the electric fields are constructively interfered, and the magnetic fields are completely suppressed by destructive interference. As a result, only electric fields induce electric dipole moment P and magnetic dipole moment M on the metasurfaces, resulting in $P = \hat{\alpha}^{ee} E^{\text{inc}}$ and $M = \hat{\alpha}^{me} E^{\text{inc}}$. Total scattered waves can be obtained by adding the scattered waves in Figs. 1(c) and 1(d):

$$S^\uparrow = S_f^+ + S_b^- = t^+ + r^- - 1, \quad (12)$$

$$S^\downarrow = S_b^+ + S_f^- = t^- + r^+ - 1, \quad (13)$$

where S^\uparrow (S^\downarrow) represents the scattered waves propagating in upward (downward) direction. The electric dipole moment P excited on the metasurface radiates in-phase electric fields whereas the magnetic dipole moment M radiates out-of-phase electric fields (or in-phase magnetic fields). In other words, a symmetric component of S^\uparrow and S^\downarrow gives electric dipole radiation, while an anti-symmetric component of S^\uparrow and S^\downarrow gives magnetic dipole radiation. Therefore, we obtain

$$\hat{\alpha}^{ee} \propto S^\uparrow + S^\downarrow = t^+ + t^- + r^+ + r^- - 2, \quad (14)$$

$$\hat{\alpha}^{me} \propto S^\uparrow - S^\downarrow = t^+ - t^- - r^+ + r^-. \quad (15)$$

Equation (14) corresponds to Eq. (2), and Eq. (15) corresponds to Eq. (5).

Contrastingly, magnetic response $P = \hat{\alpha}^{em} H^{\text{inc}}$ and $M = \hat{\alpha}^{mm} H^{\text{inc}}$ can be obtained by incident electromagnetic waves propagating in opposite directions with out-of-phase electric fields. In this case, total scattered waves can be derived by subtracting the field in Fig. 1(d) from that in Fig. 1(c):

$$S^\uparrow = S_f^+ - S_b^- = t^+ - r^- - 1, \quad (16)$$

$$S^\downarrow = S_b^+ - S_f^- = -t^- + r^+ + 1. \quad (17)$$

A symmetric component of Eqs. (16) and (17) gives electric dipole radiation, whereas an anti-symmetric component gives magnetic dipole radiation. Therefore, we acquire

$$\hat{\alpha}^{\text{em}} \propto S^\uparrow + S^\downarrow = t^+ - t^- + r^+ - r^-, \quad (18)$$

$$\hat{\alpha}^{\text{mm}} \propto S^\uparrow - S^\downarrow = t^+ + t^- - r^+ - r^- - 2. \quad (19)$$

Equation (18) corresponds to Eq. (4) whereas Eq. (19) correspond to Eq. (3).

2.3. Classification of bianisotropic metasurfaces

Reciprocity in the bianisotropic metasurfaces requires the following relations [3]:

$$\hat{\alpha}_{xx}^{\text{em}} = -\hat{\alpha}_{xx}^{\text{me}}, \quad \hat{\alpha}_{yy}^{\text{em}} = -\hat{\alpha}_{yy}^{\text{me}}, \quad \hat{\alpha}_{xy}^{\text{em}} = -\hat{\alpha}_{yx}^{\text{me}}, \quad \hat{\alpha}_{yx}^{\text{em}} = -\hat{\alpha}_{xy}^{\text{me}}. \quad (20)$$

Uniaxial metasurfaces with magneto-electric interactions can be classified into four categories in terms of non-reciprocity and polarization rotation as shown in Table 1 [4]. In the following, we briefly explain each category.

Table 1. Classification of bianisotropic metasurfaces

	Reciprocal	Non-reciprocal
With polarization rotation	Chiral with $\tilde{t}_{yx}^+ \neq \tilde{t}_{yx}^-$	Tellegen with $\tilde{r}_{yx}^+ \neq \tilde{r}_{yx}^-$
Without polarization rotation	Omega with $\tilde{r}_{xx}^+ \neq \tilde{r}_{xx}^-$	Moving with $\tilde{t}_{xx}^+ \neq \tilde{t}_{xx}^-$

A reciprocal metasurface with polarization rotation is referred to as a chiral metasurface. In the chiral metasurface, the uniaxial structure and the reciprocity require transmission coefficients \tilde{t}_{yx}^\pm to be

$$\tilde{t}_{yx}^+ - \tilde{t}_{yx}^- = -j\omega(\hat{\alpha}_{yy}^{\text{em}} - \hat{\alpha}_{xx}^{\text{me}}) = -j\omega(\hat{\alpha}_{yy}^{\text{em}} - \hat{\alpha}_{yy}^{\text{me}}) \neq 0. \quad (21)$$

Equation (21) indicates the optical activity, in which the transmission coefficients depend on propagation direction, and the polarization rotation is reversed for opposite propagating waves. Note that magnetized media or media under magnetic fields could show similar polarization rotation in transmission, known as the MO Faraday effects, with $\tilde{t}_{yx}^+ \propto \hat{\alpha}_{yx}^{\text{ee}}$ or $\tilde{t}_{yx}^+ \propto \hat{\alpha}_{yx}^{\text{mm}}$. However, these non-reciprocal MO effects do not show propagation direction dependence with respect to polarization rotation direction.

The reflection coefficients with polarization rotation, \tilde{r}_{yx}^\pm , lead to

$$\tilde{r}_{yx}^+ - \tilde{r}_{yx}^- = -j\omega(\hat{\alpha}_{yy}^{\text{em}} + \hat{\alpha}_{xx}^{\text{me}}) = -j\omega(\hat{\alpha}_{yy}^{\text{em}} + \hat{\alpha}_{yy}^{\text{me}}). \quad (22)$$

Equation (22) becomes zero for the reciprocal chiral metasurfaces due to $\hat{\alpha}_{yy}^{\text{em}} = -\hat{\alpha}_{yy}^{\text{me}}$ as in Eq. (20), but could be non-zero for non-reciprocal ones. When we compare reflection coefficients between x -polarized and y -polarized waves propagating in $+z$ direction without magneto-optical effects, we obtain $\tilde{r}_{yx}^+ = -j\omega(\hat{\alpha}_{yy}^{\text{em}} + \hat{\alpha}_{xx}^{\text{me}}) = -\tilde{r}_{xy}^+$. The non-reciprocal metasurface with polarization rotation in reflection is referred to as a Tellegen metasurface, named after Bernard Tellegen [41]. In reflection, the Tellegen metasurface shows polarization rotation in the same direction independent of polarization directions [4]. This is a non-reciprocal phenomenon with the broken time-reversal symmetry; therefore, the Tellegen metasurface seems to be similar to MO media mentioned in the above. However, the Tellegen metasurface does not show any polarization rotations in the transmission.

The reflection coefficients without polarization rotation have the following relation,

$$\tilde{r}_{xx}^+ - \tilde{r}_{xx}^- = -j\omega(\hat{\alpha}_{xy}^{\text{em}} - \hat{\alpha}_{yx}^{\text{me}}). \quad (23)$$

Equation (23) becomes non-zero even in reciprocal metasurfaces due to $\hat{\alpha}_{xy}^{\text{em}} = -\hat{\alpha}_{yx}^{\text{me}}$ as in Eq. (20). In this case, reflection coefficients without polarization rotation depend on incident direction [12], and the metasurface with $\tilde{r}_{xx}^+ \neq \tilde{r}_{xx}^-$ is referred to as an omega metasurface, which is typically observed with omega-shaped metallic structures, such as SRRs.

The transmission coefficients without polarization rotation have the following relation,

$$\tilde{t}_{xx}^+ - \tilde{t}_{xx}^- = -j\omega(\hat{\alpha}_{xy}^{\text{em}} + \hat{\alpha}_{yx}^{\text{me}}), \quad (24)$$

which is always zero for reciprocal metasurfaces represented by $\hat{\alpha}_{xy}^{\text{em}} = -\hat{\alpha}_{yx}^{\text{me}}$ as in Eq. (20), and could be non-zero for non-reciprocal metasurfaces. The symmetric off-diagonal parts in magneto-electric interactions, i.e., $\hat{\alpha}_{xy}^{\text{em}} = \hat{\alpha}_{yx}^{\text{me}} \neq 0$ causes directional-dependent transmission coefficients, which correspond to the MCh effect. The metasurface with $\tilde{t}_{xx}^+ \neq \tilde{t}_{xx}^-$ is called a moving metasurface, which exhibits an electromagnetic response equivalent to that of a regular material moving at a relativistic speed.

3. Numerical simulation setup

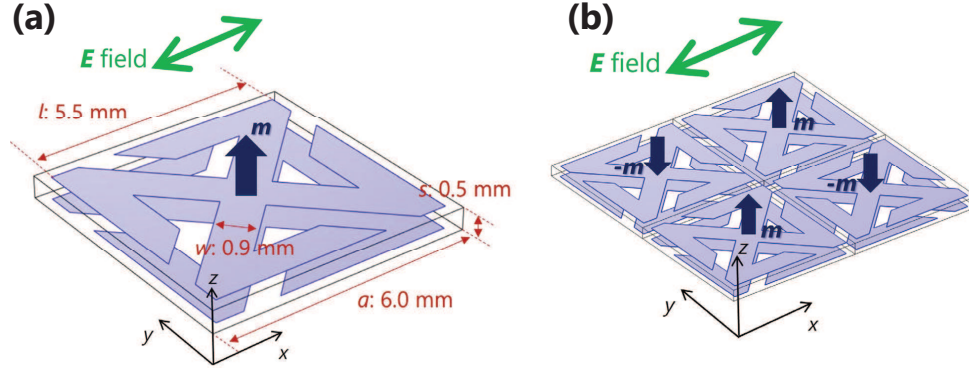


Fig. 2. (a) A unit cell of a calculated MCh metasurface consisting of $5.5 \text{ mm} \times 5.5 \text{ mm}$ Z-type gammadions on the both sides of a 0.5 mm -thick substrate. The substrate is magnetized in the $+z$ direction. The electric field of the incident microwave is polarized along the x direction. (b) A unit cell of a calculated composite metasurface including ordinary and contra-position MCh metasurfaces.

Figure 2(a) illustrates a unit cell of the uniaxial metasurface in this study. The metasurface consists of Z-type gammadions with $l = 5.5 \text{ mm}$ on the both sides of a substrate with $s = 0.5 \text{ mm}$. The design of the double Z-type gammadions are the same as those studied in Ref. [17]. The gammadions are made of perfect electric conductor with $w = 0.9 \text{ mm}$, and in the unit cell with $a = 6.0 \text{ mm}$, which is repeated in the x and y directions by a periodic boundary condition. The substrate is magnetized in the $+z$ direction. The relative electric permittivity of the substrate is constant ($\epsilon_r = 3.3$). Contrastingly, the relative magnetic permeability expressed by a tensor μ_r is varied to express the magnetized substrates. The permeability tensor μ_r for lossless substrates is described by

$$\mu_r = \begin{bmatrix} 1 & jm & 0 \\ -jm & 1 & 0 \\ 0 & 0 & 1 \end{bmatrix}, \quad (25)$$

where a parameter denoted by m is related to magnetization of the substrates. The substrate is non-magnetic when $m = 0$. On the other hand, $m > 0$ correspond to magnetic substrates

magnetized in the $+z$ direction indicated as a navy arrow in Fig. 2(a). Non-zero m causes non-zero off-diagonal components in μ_r , resulting in MO effects.

The S -parameters for microwave transmission and reflection are numerically calculated using RF module of COMSOL Multiphysics. The metasurface in the x - y plane is placed at $z = 0$ in a vacuum ranging from $z = +15$ mm to $z = -15$ mm. Ports 1 and 3 are set at $z = +15$ mm, while ports 2 and 4 are set at $z = -15$ mm. The calculation space is terminated by 15 mm-long perfect matching layers at the both ends of the vacuum. The microwaves in a frequency range between 4 and 16 GHz propagate in $-z$ direction from port 1 to the metasurface. Incident microwave is linearly polarized along the x -direction as indicated by a green arrow in Fig. 2(a). We numerically calculate S_{11} detected by port 1 corresponding to reflection with x -polarization, S_{21} detected by port 2 corresponding to transmission with x -polarization, S_{31} detected by port 3 corresponding to reflection with y -polarization, and S_{41} detected by port 4 corresponding to transmission with y -polarization.

The S -parameters S_{11} , S_{21} , S_{31} , and S_{41} are converted to reflection and transmission coefficients of the metasurface by using $r_{xx}^- = S_{11}e^{jk_0d}$, $t_{xx}^- = S_{21}e^{jk_0d}$, $r_{yx}^- = S_{31}e^{jk_0d}$, and $t_{yx}^- = S_{41}e^{jk_0d}$, where k_0 is the wavenumber in a vacuum and d is the distance between port 1(3) and port 2(4). In the same fashion, reflection and transmission coefficients for incident waves propagating in the $+z$ direction can be calculated. By using these coefficients, we obtain each component of the effective polarizability tensor.

4. Results and discussion

4.1. Transmission and reflection spectra of chiral and magnetochiral metasurfaces

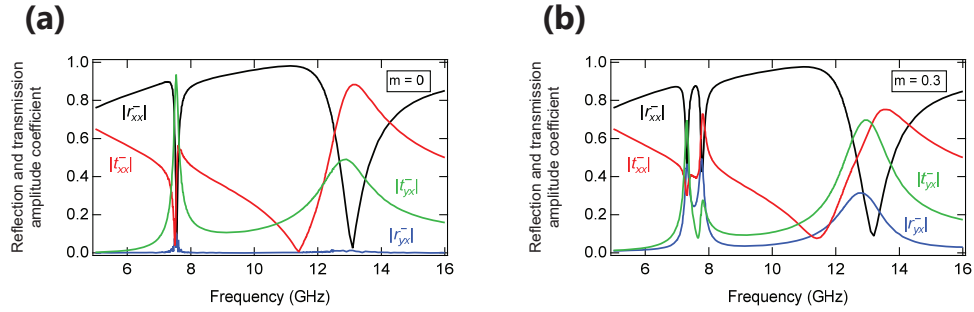


Fig. 3. Calculated spectra of $|r_{xx}^-|$ (black), $|t_{xx}^-|$ (red), $|r_{yx}^-|$ (blue), and $|t_{yx}^-|$ (green) in a frequency range of 4-16 GHz with (a) $m = 0$ and (b) $m = 0.3$.

Figure 3(a) presents calculated transmission and reflection amplitude spectra of $|r_{xx}^-|$ (black), $|t_{xx}^-|$ (red), $|r_{yx}^-|$ (blue), and $|t_{yx}^-|$ (green) in a frequency region of 4-16 GHz for a chiral metasurface with $m = 0$. $|r_{yx}^-|$ is almost zero in this frequency region. In the $|r_{xx}^-|$ spectrum, a sharp dip appears at 7.5 GHz, while a broad dip appears at 13.1 GHz. At each frequency, $|t_{xx}^-|$ spectrum exhibits dispersion-type features. These are caused by resonances by the double Z-type gammadions. The resonance in the gammadion structures results in polarization rotation of linearly polarized microwave, i.e., optical activity. Indeed, in Fig. 3(a), the $|t_{yx}^-|$ spectrum presents a sharp peak at 7.5 GHz, and a broad peak at 13.1 GHz, highlighting the optical activity by the double Z-type gammadions [17].

Figure 3(b) shows calculated spectra of $|r_{xx}^-|$ (black), $|t_{xx}^-|$ (red), $|r_{yx}^-|$ (blue), and $|t_{yx}^-|$ (green) for an MCh metasurface with $m = 0.3$. In contrast to Fig. 3(a), $|r_{yx}^-|$ in Fig. 3(b) shows peaks at approximately 7.5 and 13.1 GHz. In all spectra, the resonant mode around 7.5 GHz is split into

two mods at 7.3 and 7.8 GHz. By introducing perpendicular magnetization in the substrate, the MCh effect is induced. To verify the MCh effect, we calculate transmission phase spectra.

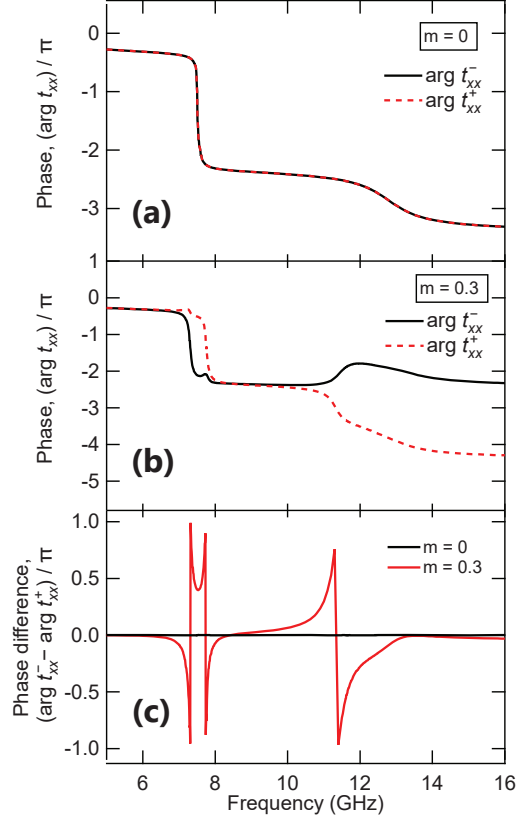


Fig. 4. Calculated spectra of $(\arg t_{xx}^-)/\pi$ (black solid) and $(\arg t_{xx}^+)/\pi$ (red dashed) with (a) $m = 0$ and (b) $m = 0.3$ in a frequency range of 4-16 GHz. (c) $(\arg t_{xx}^- - \arg t_{xx}^+)/\pi$ spectra with $m = 0$ (black) and $m = 0.3$ (red).

Figure 4(a) presents phase spectra of the chiral metasurface with $m = 0$. The phase spectrum $(\arg t_{xx}^-)/\pi$ (black solid) corresponds to the transmission in the $-z$ direction while $(\arg t_{xx}^+)/\pi$ (red dashed) corresponds to the transmission in the $+z$ direction. In Fig. 4(a), $(\arg t_{xx}^-)/\pi$ and $(\arg t_{xx}^+)/\pi$ are identical, although the phase shift is observed at 7.5 GHz and 13.1 GHz due to resonances in the gammadion structures. However, by introducing magnetization with $m = 0.3$, a phase difference appears as in Fig. 4(b). In Fig. 4(b), $(\arg t_{xx}^-)/\pi$ (black solid) is different from $(\arg t_{xx}^+)/\pi$ (red dashed) in regions of 7-8 GHz and 10-13 GHz. Figure 4(c) represents directional phase difference spectra $(\arg t_{xx}^- - \arg t_{xx}^+)/\pi$ with $m = 0$ (black) and $m = 0.3$ (red). While no phase difference is observed with $m = 0$, a large phase difference is observed with $m = 0.3$. The phase difference indicates that the MCh effect is induced in the double Z-type gammadions with perpendicular magnetization.

4.2. Effective polarizability tensor of chiral metasurfaces

The computed transmission and reflection coefficients are transformed to effective polarizabilities. Figure 5 shows frequency spectra of the extracted effective polarizabilities of the chiral metasurface with $m = 0$. Solid and dotted lines correspond to the real and imaginary parts,

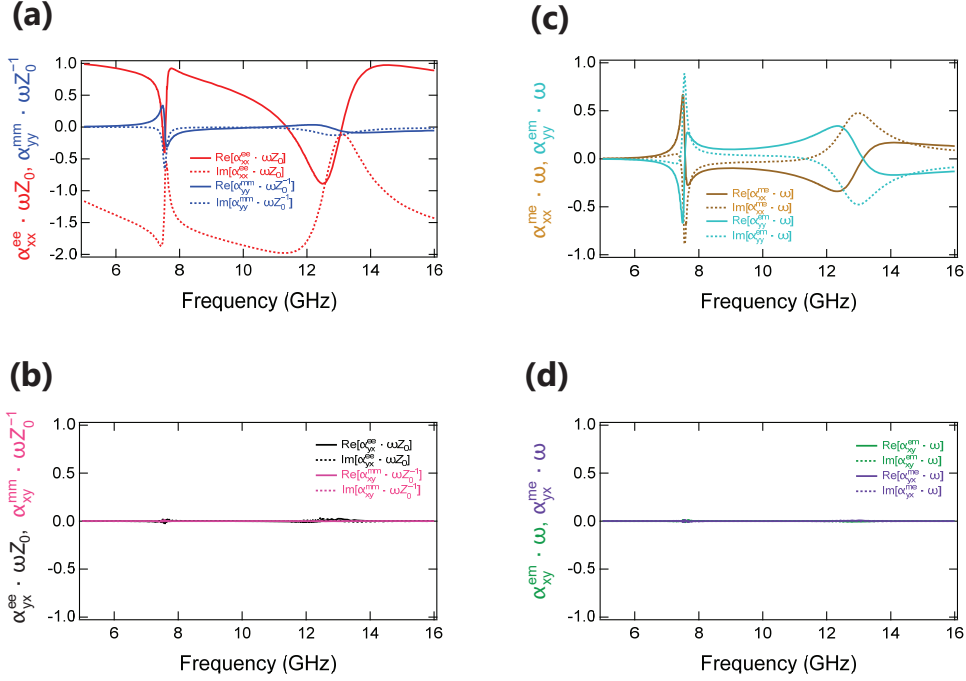


Fig. 5. Effective polarizabilities of chiral metasurfaces with $m = 0$ evaluated from numerical simulation. Frequency versus extracted (a) $\alpha_{xx}^{ee}\omega Z_0$ (red) and $\alpha_{yy}^{mm}\omega Z_0^{-1}$ (blue), (b) $\alpha_{yx}^{ee}\omega Z_0$ (black) and $\alpha_{xy}^{mm}\omega Z_0^{-1}$ (pink), (c) $\alpha_{xx}^{me}\omega$ (gold) and $\alpha_{yy}^{em}\omega$ (cyan), (d) $\alpha_{xy}^{em}\omega$ (green) and $\alpha_{yx}^{me}\omega$ (purple). Solid and dotted lines correspond to real and imaginary parts, respectively.

respectively. In Fig. 5(a), $\alpha_{xx}^{ee}\omega Z_0$ (red) corresponds to the diagonal part of electric susceptibility while $\alpha_{yy}^{mm}\omega Z_0^{-1}$ (blue) corresponds to the diagonal part of magnetic susceptibility. The $\alpha_{xx}^{ee}\omega Z_0$ spectrum representing electric dipole oscillation exhibits a sharp resonance feature at 7.5 GHz and broad feature at 13 GHz. The $\alpha_{yy}^{mm}\omega Z_0^{-1}$ spectrum representing magnetic dipole oscillation exhibits a sharp resonance at 7.5 GHz and very broad feature at 13 GHz. Figure 5(a) demonstrates that electric dipole oscillation is dominant at 13 GHz although magnetic dipole coexist.

Figure 5(b) presents the off-diagonal part of electric susceptibility, $\alpha_{yx}^{ee}\omega Z_0$ (black), and of magnetic susceptibility, $\alpha_{xy}^{mm}\omega Z_0^{-1}$ (pink). The spectra of $\alpha_{yx}^{ee}\omega Z_0$ and $\alpha_{xy}^{mm}\omega Z_0^{-1}$ indicate that the double Z-type gammadian with a non-magnetic substrate has no MO effects. In Fig. 5(c), $\alpha_{xx}^{me}\omega$ (gold) and $\alpha_{yy}^{em}\omega$ (cyan) correspond to chiral or Tellegen components. The effective polarizabilities $\alpha_{xx}^{me}\omega$ and $\alpha_{yy}^{em}\omega$ show resonant features at 7.5 and 13 GHz. We notice here $\alpha_{xx}^{me} = -\alpha_{yy}^{em}$. Given $\alpha_{yy}^{em} = \alpha_{xx}^{em}$ due to the rotational symmetry, $\alpha_{xx}^{me} = -\alpha_{xx}^{em}$ is satisfied as Eq. (20); this is the hallmark of the reciprocal chiral-type bianisotropy. This way, Fig. 5(c) demonstrates that the double Z-type gammadian with the non-magnetic substrate shows polarization rotation by reciprocal chiral-type bianisotropy. This is consistent with the fact that $|r_{yx}^-| \approx 0$ is observed in Fig. 3(a). In Fig. 5(d), $\alpha_{xy}^{em}\omega$ (green) and $\alpha_{yx}^{me}\omega$ (purple) correspond to omega or moving components. Figure 5(d) point out that moving and omega components are absent.

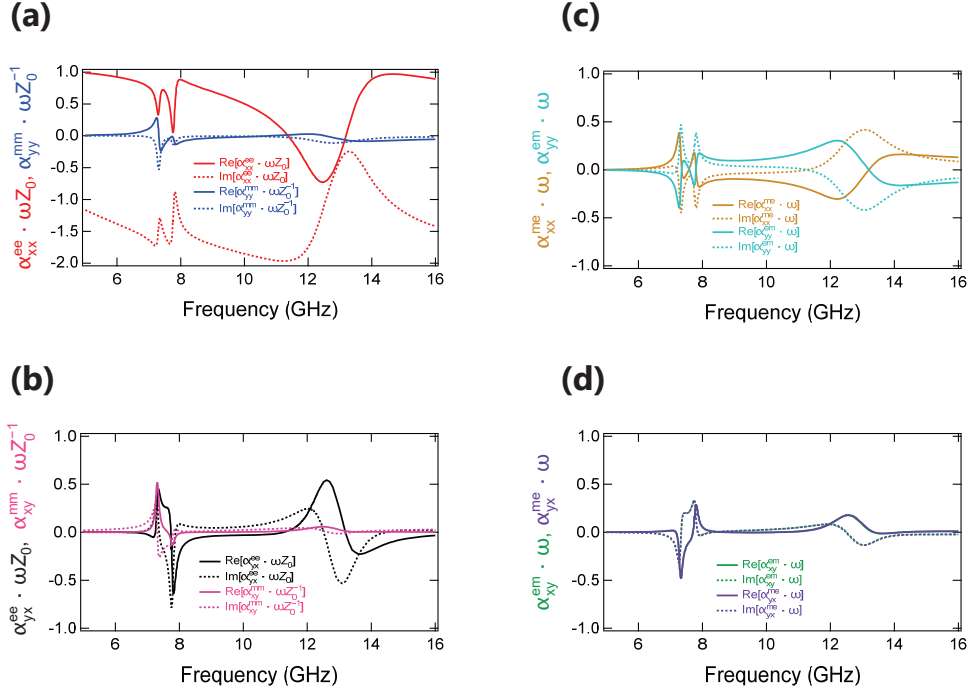


Fig. 6. Effective polarizabilities of magnetochiral metasurfaces with $m = 0.3$ evaluated from numerical simulation. Frequency versus extracted (a) $\alpha_{xx}^{ee}\omega Z_0$ (red) and $\alpha_{yy}^{mm}\omega Z_0^{-1}$ (blue), (b) $\alpha_{yx}^{ee}\omega Z_0$ (black) and $\alpha_{xy}^{mm}\omega Z_0^{-1}$ (pink), (c) $\alpha_{xx}^{me}\omega$ (gold) and $\alpha_{yy}^{em}\omega$ (cyan), (d) $\alpha_{xy}^{em}\omega$ (green) and $\alpha_{yx}^{me}\omega$ (purple). Solid and dotted lines correspond to real and imaginary parts, respectively.

4.3. Effective polarizability tensor of magnetochiral metasurfaces

Figure 6 shows extracted effective polarizabilities of the MCh metasurface with $m = 0.3$. Solid and dotted lines correspond to real and imaginary parts, respectively. Figure 6(a) presents that the resonant mode originally at 7.5 GHz with $m = 0$ is split into two modes at 7.3 and 7.8 GHz with $m = 0.3$. Figure 6(c) presents that the double Z-type gammadion with perpendicularly magnetized substrate exhibits reciprocal chiral-type bianisotropy, i.e., optical activity at 7.3, 7.8 and 13 GHz, which is similar to Fig. 5(c). Contrastingly, by introducing magnetization in the substrate, Figs. 6(b) and 6(d) are much different from Fig. 5(b) and Fig. 5(d).

In Fig. 6(b), the off-diagonal part of electric susceptibility $\alpha_{yx}^{ee}\omega Z_0$ (black) and that of magnetic susceptibility $\alpha_{xy}^{mm}\omega Z_0^{-1}$ (pink) present resonant features at approximately 7.5 and 13 GHz, indicating the MO effects due to the time-reversal symmetry breaking. Moreover, Fig. 6(d) shows non-zero $\alpha_{xy}^{em}\omega$ (green) and $\alpha_{yx}^{me}\omega$ (purple), which correspond to moving or omega-type bianisotropy. Equation (20), i.e., $\alpha_{xy}^{em}\omega = \alpha_{yx}^{me}\omega$ is satisfied in Fig. 6(d); therefore, the resonant features at 7.5 and 13 GHz are originated from the non-reciprocal moving-type bianisotropy. Effective polarizability tensor analysis shown in Fig. 6 reveals that the double Z-type gammadion with the perpendicularly magnetized substrate exhibits non-reciprocal moving-type bianisotropy without polarization rotation as well as optical activity and MO effect involving polarization rotation. The non-reciprocal moving-type bianisotropy observed in Fig. 6(d) includes cascaded MCh effect [28], which is a combination of the optical activity and MO effect.

4.4. Pure moving optical media with composite magnetochiral metasurfaces

To obtain pure moving metasurfaces, we combine the ordinary MCh metasurfaces studied in the above with contraposition MCh metasurfaces having both double inverse-Z-type gammadions and oppositely magnetized substrates. Figure 2(b) illustrates a unit cell of the composite metasurfaces consisting of ordinary and contraposition MCh metasurfaces. The optical activity is cancelled by introducing contraposition MCh metasurfaces with double inverse-Z-type gammadion having inverse chirality into the composite, similar to racemate of chiral chemical compounds. Additionally, as shown in Fig. 2(b), the contraposition metasurfaces have inverse magnetization in the $-z$ direction while the ordinary metasurfaces have magnetization in the $+z$ direction. Therefore, the MO effect by the $-z$ direction magnetization cancels out the MO effect by the $+z$ direction magnetization, similar to antiferromagnets. Nevertheless, the MCh effect is an odd function of chirality and magnetization direction; therefore, the contraposition metasurfaces has the identical sign of the MCh effect with the ordinary metasurfaces. This way, combination between ordinary and contraposition MCh metasurfaces is anticipated to exhibit a pure moving effect with neither the optical activity nor MO effect.

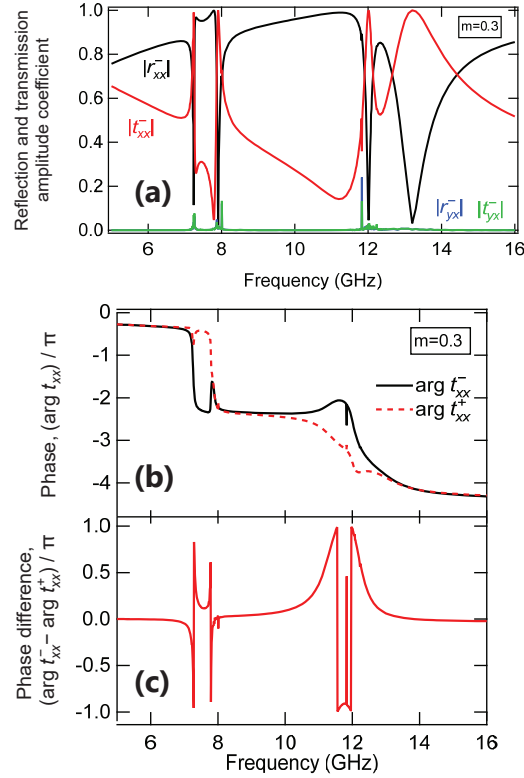


Fig. 7. (a) Calculated spectra in a frequency range of 4-16 GHz of $|r_{xx}^-|$ (black), $|t_{xx}^-|$ (red), $|r_{yx}^-|$ (blue), and $|t_{yx}^-|$ (green) for a composite MCh metasurface consisting of the ordinary MCh metasurfaces with $m = +0.3$ and contraposition MCh metasurfaces with $m = -0.3$. (b) Calculated spectra of $(\arg t_{xx}^-) / \pi$ (black solid) and $(\arg t_{xx}^+) / \pi$ (red dashed), and (c) $(\arg t_{xx}^- - \arg t_{xx}^+) / \pi$ in a frequency range of 4-16 GHz for the composite MCh metasurface.

Figure 7(a) presents calculated spectra of $|r_{xx}^-|$ (black), $|t_{xx}^-|$ (red), $|r_{yx}^-|$ (blue), and $|t_{yx}^-|$

(green) of the composite MCh metasurface with $m = \pm 0.3$ in a frequency range of 4-16 GHz. In Fig. 7(a), $|r_{xx}^-|$ (black) and $|t_{xx}^-|$ (red) show resonant features at 7.2, 7.8, 12.0, and 13.2 GHz. Moreover, $|r_{yx}^-|$ (blue) and $|t_{yx}^-|$ (green) accompanied by polarization rotation are almost zero, indicating that both the chiral-type bianisotropy and MO effect with polarization rotation are no longer functioning in the composite metasurface. Contrastingly, the moving-type bianisotropy survives as shown in Figs. 7(b) and 7(c). Figure 7(b) shows transmission phase spectra of $(\arg t_{xx}^-)/\pi$ (black solid) and $(\arg t_{xx}^+)/\pi$ (red dashed) of the composite metasurfaces. Phase differences are observed at approximately 7.5 GHz and 12 GHz. The directional phase difference spectrum, $(\arg t_{xx}^- - \arg t_{xx}^+)/\pi$, plotted in Fig. 7(c) demonstrates the moving-type bianisotropy at approximately 7.5 GHz and 12 GHz.

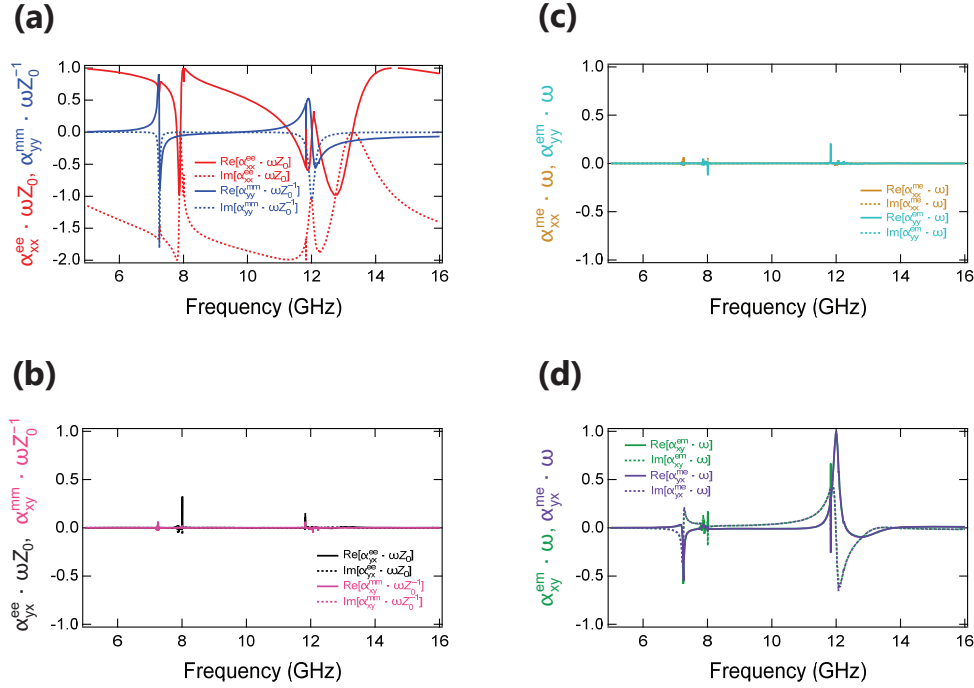


Fig. 8. Effective polarizabilities of composite MCh metasurfaces evaluated from numerical simulation. Frequency versus extracted (a) $\alpha_{xx}^{ee}\omega Z_0$ (red) and $\alpha_{yy}^{mm}\omega Z_0^{-1}$ (blue), (b) $\alpha_{yx}^{ee}\omega Z_0$ (black) and $\alpha_{xy}^{mm}\omega Z_0^{-1}$ (pink), (c) $\alpha_{xx}^{me}\omega$ (gold) and $\alpha_{yy}^{em}\omega$ (cyan), (d) $\alpha_{xy}^{em}\omega$ (green) and $\alpha_{yx}^{me}\omega$ (purple) of the composite metasurfaces consisting of ordinary MCh metasurfaces with $m = +0.3$ and contraposition MCh metasurfaces with $m = -0.3$. Solid and dotted lines correspond to real and imaginary parts, respectively.

The survival of the moving-type bianisotropy is confirmed by effective polarizability tensor. Figure 8 shows extracted (a) $\alpha_{xx}^{ee}\omega Z_0$ (red) and $\alpha_{yy}^{mm}\omega Z_0^{-1}$ (blue), (b) $\alpha_{yx}^{ee}\omega Z_0$ (black) and $\alpha_{xy}^{mm}\omega Z_0^{-1}$ (pink), (c) $\alpha_{xx}^{me}\omega$ (gold) and $\alpha_{yy}^{em}\omega$ (cyan), (d) $\alpha_{xy}^{em}\omega$ (green) and $\alpha_{yx}^{me}\omega$ (purple) of the composite MCh metasurface with $m = \pm 0.3$. Magnetic dipole represented by $\alpha_{yy}^{mm}\omega Z_0^{-1}$ in Fig. 8(a) shows a sharp resonant feature at 12 GHz compared to the ordinary MCh metasurfaces shown in Figs. 6(a). The MO effect and chiral-type bianisotropy are eliminated as in Fig. 8(b) and (c), respectively. Contrastingly and most strikingly, Fig. 8(d) demonstrates the moving-type bianisotropy. The optical moving effect at 12 GHz is much more enhanced than that at 7.5 GHz.

The transmission and reflection amplitude spectra in Fig. 7(a) show that perfect transmission and no reflection are achieved at 12 GHz, indicating the impedance matching. The impedance

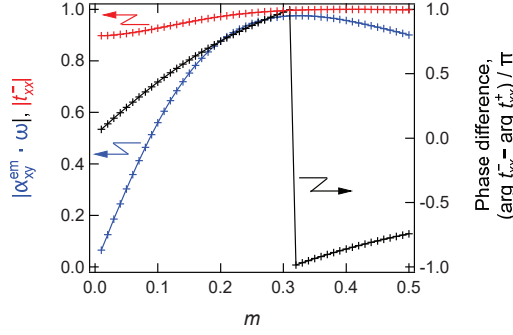


Fig. 9. $|\alpha_{xy}^{\text{em}}\omega|$ (blue, left axis), $|t_{xx}^-|$ (red, left axis), and $(\arg t_{xx}^- - \arg t_{xx}^+)/\pi$ (black, right axis) at 12.0 GHz are plotted as a function of m from 0 to 0.5.

matching is expressed as $\text{Re}[\alpha_{xx}^{\text{ee}}\omega Z_0] = \text{Re}[\alpha_{yy}^{\text{mm}}\omega Z_0^{-1}]$ and $\text{Im}[\alpha_{xx}^{\text{ee}}\omega Z_0] = \text{Im}[\alpha_{yy}^{\text{mm}}\omega Z_0^{-1}]$, corresponding to Kerker condition [42], which is satisfied at 12 GHz in Fig. 8(a). We notice in Fig. 8(d) that $|\alpha_{xy}^{\text{em}}\omega|$ is maximized, i.e., $|\alpha_{xy}^{\text{em}}\omega| = 1$, at 12 GHz. The maximized $|\alpha_{xy}^{\text{em}}\omega| = 1$ derives automatically both a perfect transparency and phase difference of π as proved in the following. In the moving medium, i.e., $\hat{\alpha}_{xy}^{\text{em}} = \hat{\alpha}_{yx}^{\text{me}}$, Eq. (24) is written as

$$\tilde{t}_{xx}^+ - \tilde{t}_{xx}^- = -2j\omega\hat{\alpha}_{xy}^{\text{em}}. \quad (26)$$

Absolute value of Eq. (26) is

$$2|\omega\hat{\alpha}_{xy}^{\text{em}}| = |\tilde{t}_{xx}^+ - \tilde{t}_{xx}^-| \leq |\tilde{t}_{xx}^+| + |\tilde{t}_{xx}^-| \leq 2. \quad (27)$$

Equation (27) highlights that the maximum value $|\alpha_{xy}^{\text{em}}\omega| = 1$ is achieved when $\tilde{t}_{xx}^+ = -\tilde{t}_{xx}^-$ and $|\tilde{t}_{xx}^\pm| = 1$. The phase difference of π , $(\arg t_{xx}^- - \arg t_{xx}^+)/\pi = 1$, is indicated at 12 GHz in Fig. 7(c).

The effective polarizability tensor $|\alpha_{xy}^{\text{em}}\omega|$, transmission coefficient $|t_{xx}^-|$, and phase difference $(\arg t_{xx}^- - \arg t_{xx}^+)/\pi$ at 12.0 GHz are calculated and evaluated with an increase in parameter m related to magnetization from $m = 0$ to 0.5. In Fig. 9, $|\alpha_{xy}^{\text{em}}\omega|$ (blue, left axis), $|t_{xx}^-|$ (red, left axis), and $(\arg t_{xx}^- - \arg t_{xx}^+)/\pi$ (black, right axis) at 12.0 GHz are plotted as a function of m . Figure 9 presents that $m = 0.31$ brings about the maximum value of $|\alpha_{xy}^{\text{em}}\omega| = 0.975$, which is accompanied by $(\arg t_{xx}^- - \arg t_{xx}^+)/\pi = 1.0$ and $|t_{xx}^-| = 1.0$. This way, the ideal gyrator for arbitrary polarizations is realized using the composite metasurface with ordinary and contraposition MCh metasurfaces. Applications of the ideal gyrator include an isolator, circulator, non-reciprocal holography [43], two-wavelength lasing [29], and artificial gauge field for light [44]. The pure moving optical medium is also relevant in fundamental physics in an analogy with a hypothetical particle called dyon [45], and from the view point of interplay between physics and mathematics in algebraic geometry with Fresnel-Kummer surfaces [46, 47].

5. Conclusion

Effective polarizability tensor is numerically evaluated to study bianisotropies in MCh metasurfaces. The ordinary MCh metasurface consisting of the double Z-type gammadions with perpendicularly magnetized substrate shows the non-reciprocal moving-type bianisotropy as well as the reciprocal chiral-type bianisotropy and non-reciprocal MO effect. The chiral-type bianisotropy and MO effect are eliminated by the combining the ordinary MCh metasurfaces with the contraposition MCh metasurfaces having inverse-Z-type gammadion and oppositely magnetized substrates. This realizes pure moving optical media. The pure moving optical

media demonstrate perfect transmission with phase difference of π , which is a key to embody an ideal gyrator for arbitrary spatial and polarization modes.

Funding. This work is financially supported by KAKENHI (23K13621) and JST-CREST (JPMJCR2102).

Acknowledgments. The authors are grateful to Y. Tamayama and T. Ueda for fruitful discussions and comments. H. Kurosawa is also acknowledged for instructing the numerical calculation prior to this work.

Disclosures. The authors declare no conflicts of interest.

Data availability. Data underlying the results presented in this paper are not publicly available at this time but may be obtained from the authors upon reasonable request.

References

1. L. D. Landau, E. M. Lifshitz, and L. P. Pitaevski, *Electrodynamics of Continuous Media (2nd edition)* (Butterworth-Heinemann, Oxford, 1984).
2. J. A. Kong, *Electromagnetic Wave Theory* (EMW Publishing, Cambridge, 2005).
3. C. Simovski and S. Tretyakov, *An introduction to Metamaterials and Nanophotonics* (Cambridge University Press, 2020).
4. V. S. Asadchy, A. Díaz-Rubio, and S. A. Tretyakov, "Bianisotropic Metasurfaces: Physics and Applications," *Nanophotonics* **7**, 1069 (2018).
5. S. Toyoda, N. Abe, S. Kimura, Y. H. Matsuda, T. Nomura, A. Ikeda, S. Takeyama, and T. Arima, "One-Way Transparency of Light in Multiferroic CuB_2O_4 ," *Phys. Rev. Lett.* **115**, 267207 (2015).
6. A. M. Kuzmenko, V. Dziom, A. Shuvaev, Anna Pimenov, M. Schiebl, A. A. Mukhin, V. Yu. Ivanov, I. A. Gudim, L. N. Bezmaternykh, and A. Pimenov, "Large directional optical anisotropy in multiferroic ferroborate," *Phys. Rev. B* **92**, 184409 (2015).
7. M. Fiebig, T. Lottermoser, D. Meier and M. Trassin, "The evolution of multiferroics," *Nat. Rev. Mater.* **1**, 16046 (2016).
8. X. Chen, B.-I. Wu, J. A. Kong, and T. M. Grzegorzczuk, "Retrieval of the effective constitutive parameters of bianisotropic metamaterials," *Phys. Rev. E* **71**, 046610 (2005).
9. N. Kida, T. Yamada, M. Konoto, Y. Okimoto, T. Arima, K. Koike, H. Akoh, and Y. Tokura, "Optical Magnetolectric Effect in a Submicron Patterned Magnet," *Phys. Rev. Lett.* **94**, 077205 (2005).
10. E. Plum, V. A. Fedotov, and N. I. Zheludev, "Extrinsic electromagnetic chirality in metamaterials," *J. Opt. A: Pure Appl. Opt.* **11**, 074009 (2009).
11. Z. Li, K. Aydin, and E. Ozbay, "Determination of the effective constitutive parameters of bianisotropic metamaterials from reflection and transmission coefficients," *Phys. Rev. E* **79**, 026610 (2009).
12. T. Niemi, A. O. Karilainen, and S. A. Tretyakov, "Synthesis of Polarization Transformers," *IEEE Trans. Antennas Propag.* **61**, 3102 (2013).
13. C. Pfeiffer, and A. Grbic, "Bianisotropic Metasurfaces for Optimal Polarization Control: Analysis and Synthesis," *Phys. Rev. Appl.* **2**, 044011 (2014).
14. C. Pfeiffer, C. Zhang, V. Ray, L. Jay Guo, and A. Grbic, "High Performance Bianisotropic Metasurfaces: Asymmetric Transmission of Light," *Phys. Rev. Lett.* **113**, 023902 (2014).
15. M. Odit, P. Kapitanova, P. Belov, R. Alaei, C. Rockstuhl, and Y. S. Kivshar, "Experimental realisation of all-dielectric bianisotropic metasurfaces," *Appl. Phys. Lett.* **108**, 221903 (2016).
16. G. Lavigne and C. Caloz, "Generalized Brewster effect using bianisotropic metasurfaces," *Opt. Express* **29**, 11361 (2021).
17. T. T. Kim, S. S. Oh, H.-S. Park, R. Zhao, S.-H. Kim, W. Choi, B. Min, and O. Hess, "Optical Activity Enhanced by Strong Inter-Molecular Coupling in Planar Chiral Metamaterials," *Sci. Reports* **4**, 5864 (2014).
18. M. P. Groenewege, "A theory of magneto-optical rotation in diamagnetic molecules of low symmetry," *Mol. Phys.* **5**, 541 (1962).
19. D. L. Portugal and E. Burstein, "Magneto-spatial dispersion effects on the propagation of electro-magnetic radiation in crystals," *J. Phys. Chem. Solids* **32**, 603 (1971).
20. N. B. Baranova, Yu. V. Bogdanov, and B. Ya. Zeldovich, "Electrical analog of the Faraday effect and other new optical effects in liquids," *Opt. Commun.* **22**, 243 (1977).
21. V. A. Markelov, M. A. Novikov, and A. A. Turkin, "Experimental observation of a new nonreciprocal magneto-optical effect," *JETP Lett.* **25**, 378 (1977) [*Pis'ma Zh. Eksp. Teor. Fiz.* **25**, 404 (1977)].
22. N. B. Baranova and B. Ya. Zeldovich, "Theory of a new linear magnetorefractive effect in liquids," *Mol. Phys.* **38**, 1085 (1979).
23. G. Wagnière and A. Meier, "The influence of a static magnetic field on the absorption coefficient of a chiral molecule," *Chem. Phys. Lett.* **93**, 78 (1982).
24. G. Wagnière, "Magnetochiral dichroism in emission. Photoselection and the polarization of transitions," *Chem. Phys. Lett.* **110**, 546 (1984).
25. L. D. Barron and J. Vrbancich, "Magneto-chiral birefringence and dichroism," *Mol. Phys.* **51**, 715 (1984).

26. G. L. J. A. Rikken and E. Raupach, "Observation of magneto-chiral dichroism," *Nature* **390**, 493 (1997).
27. P. Kleindienst and G. H. Wagnière, "Interferometric detection of magneto-chiral birefringence," *Chem. Phys. Lett.* **288**, 89 (1998).
28. G. L. J. A. Rikken and E. Raupach, "Pure and cascaded magneto-chiral anisotropy in optical absorption," *Phys. Rev. E* **58**, 5081 (1998).
29. M. Vallet, R. Ghosh, A. Le Floch, T. Ruchon, F. Bretenaker, and J.-Y. Thépot, "Observation of Magneto-chiral Birefringence," *Phys. Rev. Lett.* **87**, 183003 (2001).
30. C. Train, R. Gheorghe, V. Krstic, L.-M. Chamoreau, N. S. Ovanesyan, G. L. J. A. Rikken, M. Gruselle, and M. Verdaguer, "Strong magneto-chiral dichroism in enantiopure chiral ferromagnets," *Nat. Mater.* **7**, 729-734 (2008).
31. S. Tomita, K. Sawada, A. Porokhnyuk, and T. Ueda, "Direct Observation of Magneto-chiral Effects through a Single Metamolecule in Microwave Regions," *Phys. Rev. Lett.* **113**, 235501 (2014).
32. S. Tomita, H. Kurosawa, T. Ueda, and K. Sawada, "Metamaterials with magnetism and chirality," *J. Phys. D: Appl. Phys.* **51**, 083001 (2018).
33. M. Atzori, G. L. J. A. Rikken, and C. Train, "Magneto-Chiral Dichroism: A Playground for Molecular Chemists," *Chem. Eur. J.* **26**, 9784 (2020).
34. J. M. Caridad, C. Tserkezis, J. E. Santos, P. Plochocka, M. Venkatesan, J. M. D. Coey, N. Asger Mortensen, G. L. J. A. Rikken, and V. Krstić, "Detection of the Faraday Chiral Anisotropy," *Phys. Rev. Lett.* **126**, 177401 (2021).
35. M. S. Mirmoosa, Y. Ra'di, V. S. Asadchy, C. R. Simovski, and S. A. Tretyakov, "Polarizabilities of Nonreciprocal Bianisotropic Particles," *Phys. Rev. Appl.* **1**, 034005 (2014).
36. R. Alaei, M. Albooyeh, M. Yazdi, N. Komjani, C. Simovski, F. Lederer, and C. Rockstuhl, "Magnetolectric coupling in nonidentical plasmonic nanoparticles: Theory and applications," *Phys. Rev. B* **91**, 115119 (2015).
37. M. Yazdi and N. Komjani, "Polarizability Calculation of Arbitrary Individual Scatterers, Scatterers in Arrays, and Substrated Scatterers," *J. Opt. Soc. Am. B* **33**, 491 (2016).
38. D. M. Pozar, *Microwave Engineering, 3rd. Ed.* (Wiley, 2005).
39. D. R. Smith, J. Gollub, J. J. Mock, W. J. Padilla, and D. Schurig, "Calculation and measurement of bianisotropy in a split ring resonator metamaterial," *J. Appl. Phys.* **100**, 024507 (2006).
40. C. É. Kriegler, M. S. Rill, S. Linden, and M. Wegener, "Bianisotropic Photonic Metamaterials," *IEEE J. Sel. Top. Quantum Electron.* **16**, 367 (2010).
41. B. D. Tellegen, "The gyrator, a new electric network element," *Philips Res Rep* **3**, 81-101 (1948).
42. M. Kerker, D.-S. Wang, and C. Giles, "Electromagnetic scattering by magnetic spheres," *J. Opt. Soc. Am. A* **73**, 765 (1983).
43. W. Yang, J. Qin, J. Long, W. Yan, Y. Yang, C. Li, E. Li, J. Hu, L. Deng, Q. Du, and L. Bi, "A self-biased non-reciprocal magnetic metasurface for bidirectional phase modulation," *Nat. Electron.* **6**, 225-234 (2023).
44. K. Sawada and N. Nagaosa, "Optical Magnetolectric Effect in Multiferroic Materials: Evidence for a Lorentz Force Acting on a Ray of Light," *Phys. Rev. Lett.* **95**, 237402 (2005).
45. D. I. Khomskii, "Magnetic monopoles and unusual dynamics of magnetoelectrics," *Nat. Commun.* **5**, 4793 (2014).
46. R. W. H. T Hudson, *Kummer's Quartic Surface*, (the University Press, Cambridge, 1905).
47. A. Favaro and F. W. Hehl, "Light propagation in local and linear media: Fresnel-Kummer wave surfaces with 16 singular points," *Phys. Rev. A* **93**, 013844 (2016).